Comparison of submicron particle analysis by Auger electron spectroscopy, time-of-flight secondary ion mass spectrometry, and secondary electron microscopy with energy dispersive x-ray spectroscopy

Kenton D. Childs,[a] David Narum, and Lori A. LaVanier
Physical Electronics Inc., 6509 Flying Cloud Dr., Eden Prairie, Minnesota 55344

Patricia M. Lindley
Charles Evans & Associates, 301 Chesapeake Drive, Redwood City, California 94063

Bruno W. Schueler
Physical Electronics Inc., 575 Chesapeake Drive, Redwood City, California 94063

George Mulholland
National Institute of Standards & Technology, Gaithersburg, Maryland 20899

Alain C. Diebold
Sematech, 2706 Montopolis Drive, Austin, Texas 78741

(Received 19 October 1995; accepted 5 April 1996)

Particulate contamination can result in a significant yield loss during semiconductor device fabrication. As device design rule dimensions decrease the critical defect size also decreases, resulting in the need to analyze smaller defects. Current manufacturing requirements include analysis of sub-0.5-μm defects, with analysis of sub-0.1-μm defects expected in the near future. This article investigates the particle analysis capabilities of Auger electron spectroscopy, time-of-flight secondary ion mass spectrometry, and energy dispersive x-ray spectroscopy during scanning electron microscopy (SEM/EDS). In order to evaluate each method carefully, a standard set of samples was prepared and analyzed. These samples consist of 0.5-, 0.3-, and 0.1-μm Al and Al_2O_3 deposited on 1-in. Si wafers. Although all the methods observed an Al signal, a semiquantitative gauge of capability based on the relative strengths of particle versus substrate signal is provided. The dependence of the sample-to-substrate signal on primary electron energy is examined for both EDS and Auger analyses. The ability to distinguish metallic Al particles from Al oxide particles for the three techniques is also discussed.

I. INTRODUCTION

Particulate contamination is a major issue in semiconductor device processing and can result in a significant yield loss. Thus, finding the source of particles and eliminating them from the process is a critical activity. The ability to identify the particle composition is a key enabler when determining the source of contamination. Therefore, particle compositional analysis is done to support process/tool development, pilot line integrated circuit (IC) yield improvement, and yield improvement during volume IC manufacture.[1]

Particle compositional analysis becomes more difficult as the killer defect size decreases along with the IC design rules for each new generation of devices. Table I shows the design rule and particle size requirements for several generations of IC technology, taken from Sematech's *National Technology Roadmap for Semiconductors*,[2] and the *Metrology Supplement*.[3] These documents describe the projected needs for materials, equipment, and processes related to the semiconductor industry for the next 15 years, based on the first volume shipment of dynamic random access memory (DRAM) technology. It is worth noting that the technology requirements for the development line occur three years earlier. According to the roadmap, the critical particle size for volume shipment is currently 1200 Å, with development line requirements of 800 Å. In 1998 the critical particle size for volume shipment will be 800 Å, with development line requirements of 600 Å.

This article compares the particle analysis capabilities of energy dispersive x-ray spectroscopy on a scanning electron microscope (SEM/EDS), Auger electron spectroscopy (AES), and time-of-flight secondary ion mass spectrometry (TOF-SIMS). SEM/EDS is typically used in existing defect review tools (DRTs). AES and TOF-SIMS are two of the near term potential analysis methods listed in Sematech's *Metrology Supplement* for alternate defect characterization technologies. Analytical approaches besides EDS are being considered as it is not expected that current, high voltage (>5 keV) SEM/EDS-based technology will meet the analysis needs predicted for future IC generations.

Present x-ray detector technology limits analysis conditions, as current EDS detectors have modest energy resolution ($\Delta E \approx 50$ eV at 100–200 eV to 2–3 keV; $\Delta E = 130$ eV at 6 keV) and poor sensitivity to low energy x rays (100–200 eV to 2–3 keV). Typical particle and defect analysis is done using high accelerating voltage electron beams (>10 kV, and often >20 kV), resulting in a large sampling volume for EDS-based x-ray analysis. This is due to the inelastic scatter

[a]Electronic mail: kchilds@phi.com

TABLE I. Particle size road map for particle composition analysis.

Year of first shipment	1995	1998	2001	2004	2007	2010
IC design rule	0.35 μm	0.25 μm	0.18 μm	0.13 μm	0.10 μm	0.07 μm
Particle size	0.12 μm	0.08 μm	0.06 μm	0.04 μm	0.03 μm	0.02 μm

of electrons in the particle and sample. Characterization of small particles (sub-100-nm diameter) and defects on patterned wafers will be difficult at these electron beam energies. While lower electron beam energies result in a reduced sampling volume, the limited energy resolution of current EDS detectors is often insufficient to differentiate between low energy x-ray lines of different elements.

Three sets of reference samples were prepared for the evaluation of light element analytical capabilities using AES, TOF-SIMS, and SEM/EDS. Each set of samples consist of six 1-in. wafers, with each wafer having 0.5-, 0.3-, or 0.1-μm-diam Al or Al_2O_3 particles purposefully deposited at a high density near the center of the wafer. The objective of the sample preparation is to have samples that allow rapid location of particles at a magnification of 1000×.

II. PARTICLE DEPOSITION PROCEDURE

Particle deposition was done at the National Institute of Standards and Technology (NIST) on 2.54-cm- (1-in.-) diam silicon wafers. Particle suspensions were made of three different powders: 5 m^2/g aluminum and 5 and 14 m^2/g alumina, where the numerical designation refers to the surface area per unit mass. Suspensions of aluminum were made with isopropanol to prevent oxidation, and those of alumina were made with deionized water.

The particle deposition system consists of an aerosol generation system, a differential mobility classifier (DMA) for selecting a monodisperse size fraction, a condensation nucleus counter for monitoring the aerosol concentration, and a cascade impactor for depositing the aerosol. The particle suspension is placed in an ultrasonic bath to break up aggregate particles and then the suspension is nebulized to form a droplet aerosol with droplets containing the solid particles. The nebulizer produces a broad distribution of droplets extending from about 0.1 to 5 μm with a mass median diameter of about 3 μm. The water evaporates as the aerosol flows through a diffusion drier and is mixed with clean, dry air. The aluminum or alumina particle aerosol was charged with a bipolar charger and then electrostatically classified to produce a monodisperse aerosol of known size.

The cascade impactor consists of eight stages, each with a holder for a 25-mm-diam collection substrate. Both glass cover slips and 1-in. silicon wafers were used. The collection stage used depends on the particle density and size. In all cases, the stages preceding the collection stage were loaded with glass cover slips that had been lightly coated with a silicone grease. This prevented larger particles from bouncing off the precollection surfaces. The collection times ranged from 5 to 25 min depending on the particle type, particle concentration, and size.

After the deposition was complete, the collection disk was observed under an optical microscope where it was noted

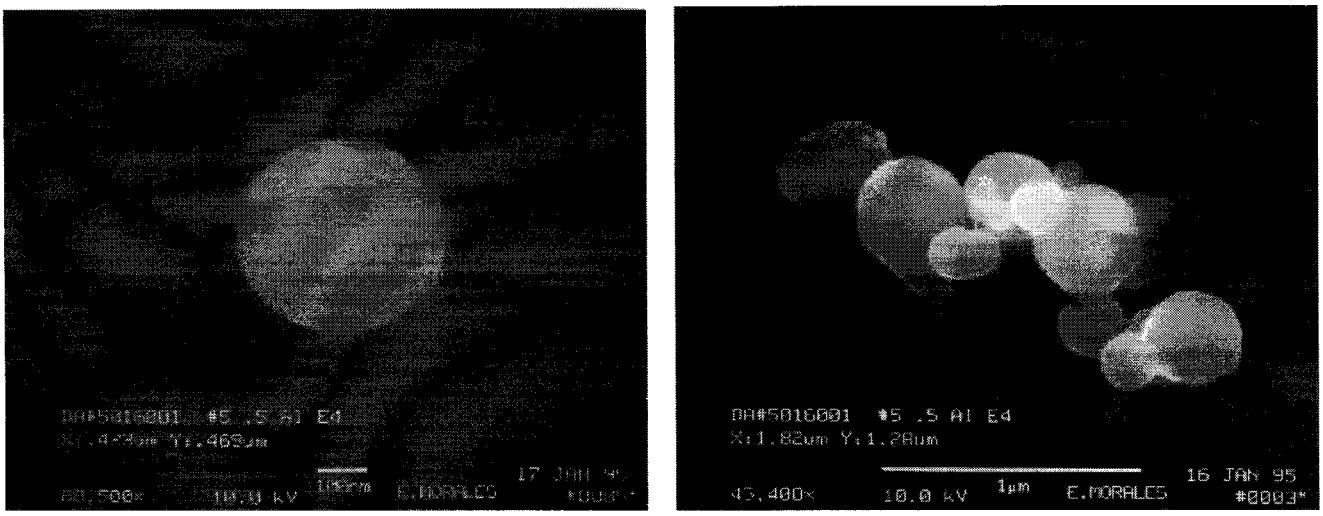

FIG. 1. Secondary electron images of typical particles analyzed with the field emission SEM/EDS. These particles are nominally 0.5 μm, but in fact vary in shape from nearly round to an agglomeration of small particles.

that the deposition had fewer multiple particles a distance of 0.5–1 mm from the center of the deposition pattern. Thus, all particle counting analyses were performed in the off-center region, which is also the region recommended for chemical analysis. The particles in one-quarter of a 1000× dark field photograph were counted to estimate the particle density. The distribution of particles on the collection disks was not uniform and often resembled a bull's-eye with a higher density of particles in the center, followed by a sparse region, and a moderate density of relatively monosized particles outside of that, which tapered off with distance from the center. A typical count for the metal powder suspensions yielded about 150 particles in a 0.01 mm^2 moderately dense area of the collection disk. This gives a particle density of 15 000/mm^2. Electron microscopy revealed a density of about 3000/mm^2 for the same sample, but not necessarily at the same location.

III. SEM/EDS ANALYSIS OF Al AND Al_2O_3 PARTICLES ON Si WAFERS

A. SEM/EDS experimental

Two different SEM/EDS systems were used to analyze the Al and Al_2O_3 particles. One SEM had a field emission electron source and was equipped with an EDS system having a Si detector with an energy resolution of $\Delta E = 154$ eV at Mn. This system was used to characterize all six samples with 5 and 10 kV primary electron beam voltages.

The second SEM had a W filament electron source and was equipped with an EDS system having a 10-mm Si de-

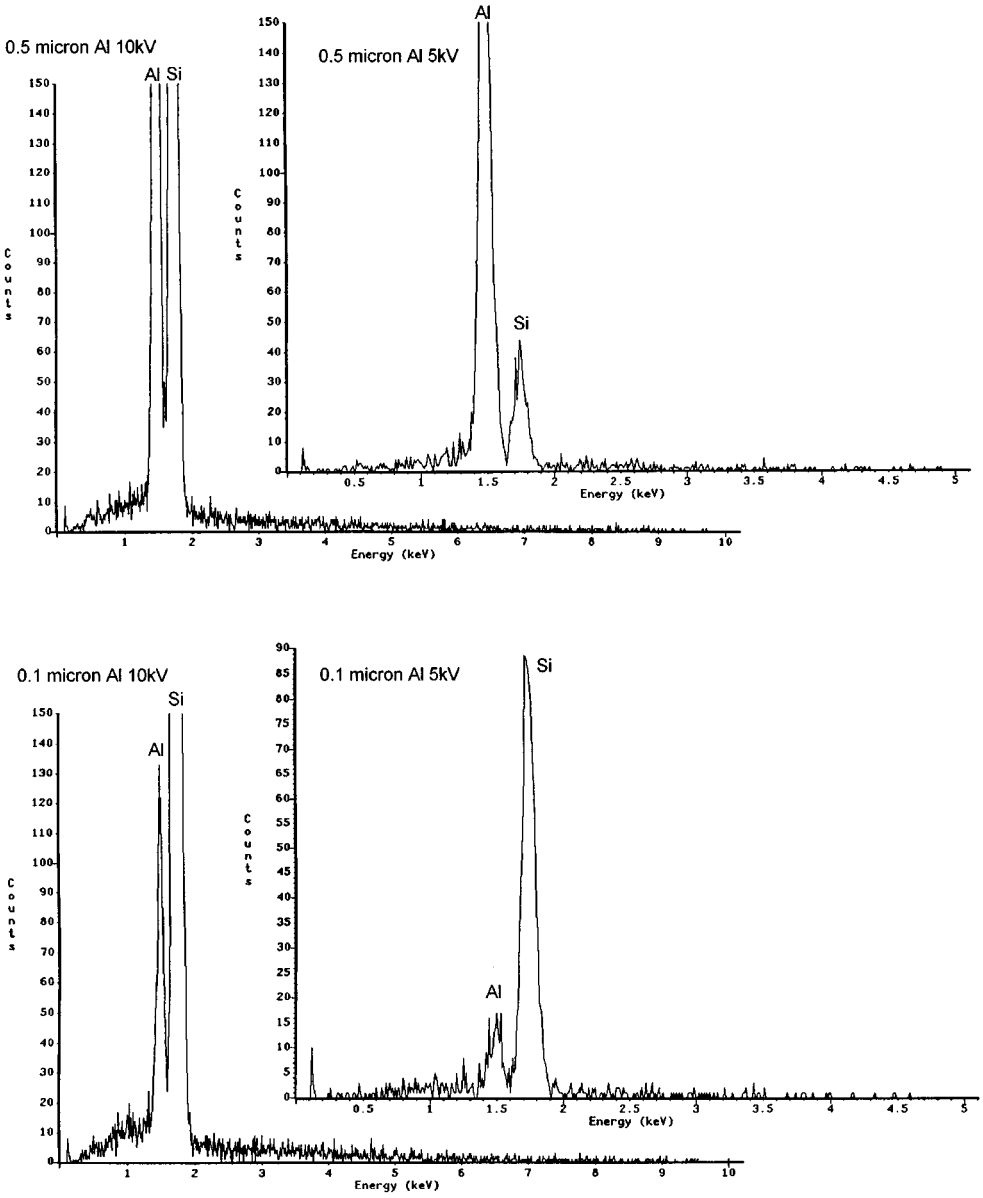

FIG. 2. Energy dispersive x-ray spectra from the field emission SEM/EDS for 0.5- and 0.1-μm Al particles, obtained with 5 and 10 kV primary beam voltages.

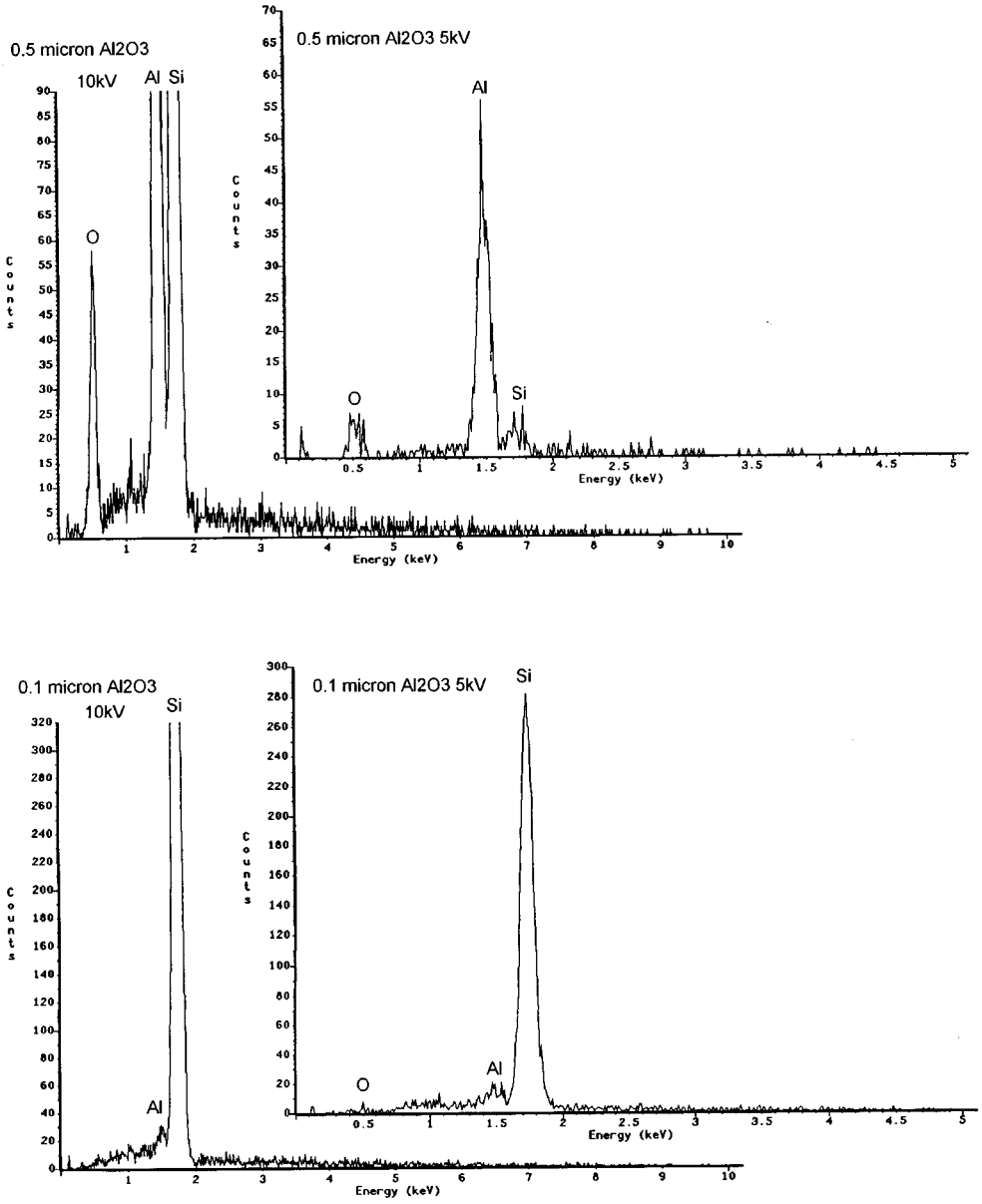

FIG. 3. Energy dispersive x-ray spectra from the field emission SEM/EDS for 0.5- and 0.1-μm Al_2O_3 particles, obtained with 5 and 10 kV primary beam voltages.

tector, an atmospheric thin window, and an energy resolution of $\Delta E = 133$ eV at Mn. This system was used to characterize the 0.5- and 0.3-μm Al particles and the 0.5-μm Al_2O_3 particles with 5, 10, and 20 kV primary electron beam voltages. EDS data for the 0.1-μm Al particle were taken using 5 and 10 kV primary electron beam voltages. The 0.3- and 0.1-μm Al_2O_3 particles were not analyzed. In the case of a W filament SEM, the electron beam size at lower voltages provided an instrumental limitation for imaging the small particles and hence for constraining the analyzed volume to the particles.

B. SEM/EDS results and discussion

X-ray spectra were obtained for multiple particles. Not all the particles analyzed by the field emission SEM were round in shape; many were irregularly shaped or consisted of an agglomeration of smaller particles. Examples of the extremes in particle shape are shown in Fig. 1. EDS analysis shows that Al is detected in all the analyzed particles for the analytical conditions described above. The Al $K\alpha$ line appears quite strong for the 0.5-μm particles, much weaker for the 0.1-μm Al particles, and very small for the 0.1-μm Al_2O_3 particles as shown in Figs. 2 and 3.

EDS analysis sometimes shows the presence of O, along with Al and Si, for the Al_2O_3 particles. The O $K\alpha$ line is clearly observed for the 0.5-μm particle, is relatively weak for the 0.3-μm particles, and is very small or not observable for the 0.1-μm Al_2O_3 particles, as shown in Fig. 3 for the 0.5- and 0.1-μm particles. Quantitative EDS analysis is complicated by the unusual electron scattering properties of ir-

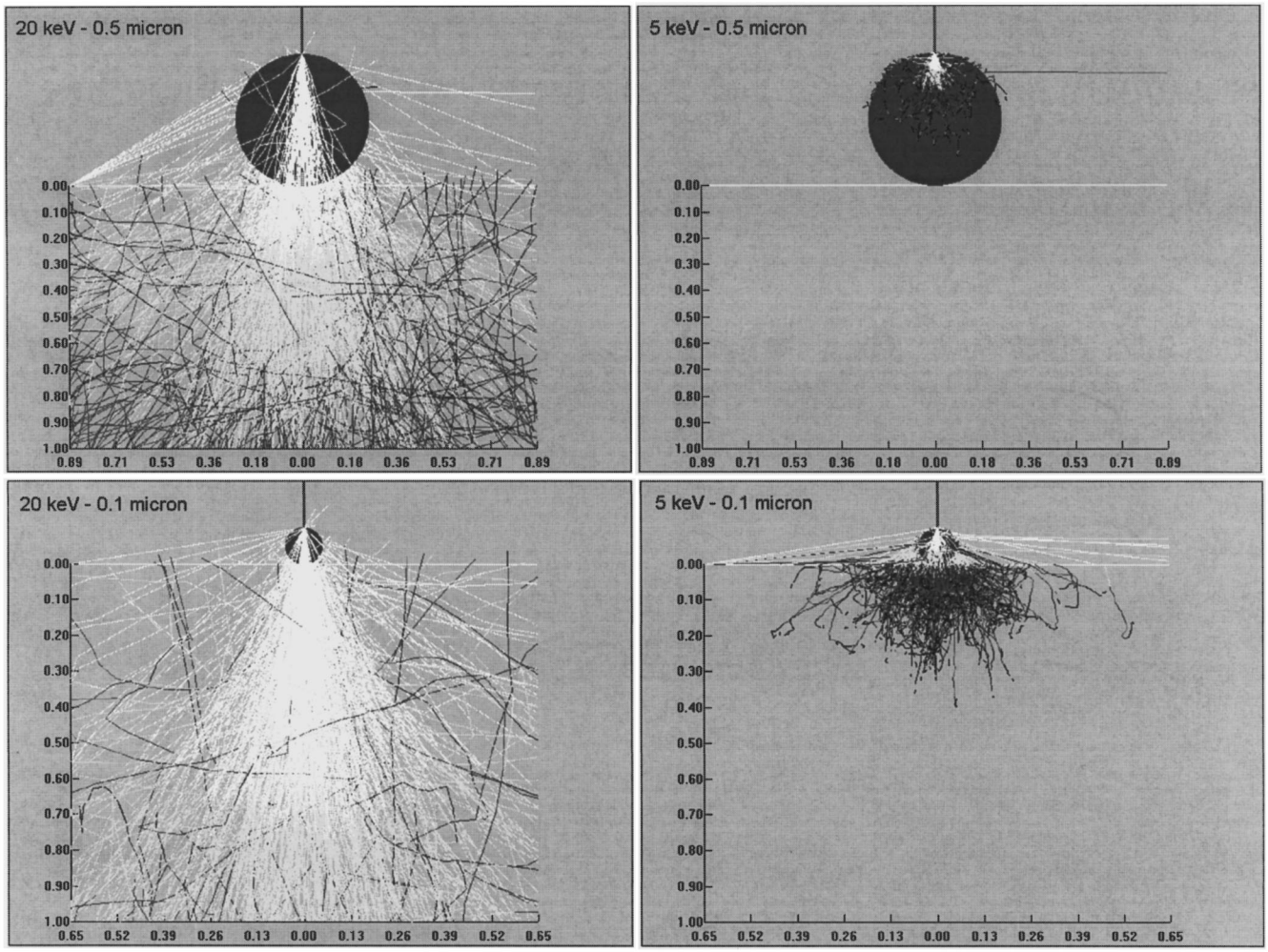

FIG. 4. Monte Carlo simulations of the electron interaction volume for 20 and 5 keV primary electrons incident on 0.5- and 0.1-μm Al particles on Si.

regularly shaped particles on a surface. Standard quantitative analysis, referenced to the supplier's standard library, yielded O:Al ratios much higher than 3:2, on the order of 2:1 to 7:1. Quantitative EDS analysis referenced to standards similar to the Al_2O_3 particles or to appropriate Monte Carlo models should yield O:Al ratios closer to the expected 3:2 value. In those cases where O is not found, quantitative analysis of Al_2O_3 is, of course, not meaningful.

The Si $K\alpha$ line from the Si substrate is also evident in all the EDS spectra and dominates the spectra for the smallest particles. The presence of Si in the x-ray spectra results from the large analyzed volume relative to the particle size. This analyzed volume results from the scattering of the primary electrons within the sample, and is dependent on primary beam voltage. Figure 4 shows the interaction volumes calculated by Monte Carlo simulations[4] for 5 and 20 keV primary electrons incident on 0.5- and 0.1-μm Al particles on Si.

One measure of the degree to which the analyzed volume is constrained to the particle is to calculate the relative contribution of the signal from the particle to that from the substrate, i.e., the Al/Si intensity ratio. Displayed in Figs. 5 and 6 are plots of the average EDS Al/Si intensity ratio for each particle size as a function of primary beam voltage for the Al and Al_2O_3 particles, respectively. The error bars represent the range of ratios which resulted from at least five measurements. The solid data points indicate the average value at each primary beam voltage. Note that the scatter in the EDS ratios for a single particle size at a given beam voltage is often on the order of the average value. This results in large uncertainties in the Al/Si ratio, especially for 5 kV beam voltages. The scatter in Al/Si intensities may be partially due to the variety of particle shapes that were measured. These plots indicate that for all particle sizes, a lower beam voltage (5 kV) gives a greater EDS Al/Si ratio over the limited beam voltage range for which EDS spectra were acquired.

IV. AES ANALYSIS OF Al AND Al_2O_3 PARTICLES ON Si WAFERS

A. AES experiment

Auger analysis of the Al and Al_2O_3 particles on 1-in.-diam silicon wafers was performed with a Physical Electronics Model 670*xi* scanning Auger nanoprobe. This system uses a cylindrical mirror analyzer (CMA) with a coaxial Schottky

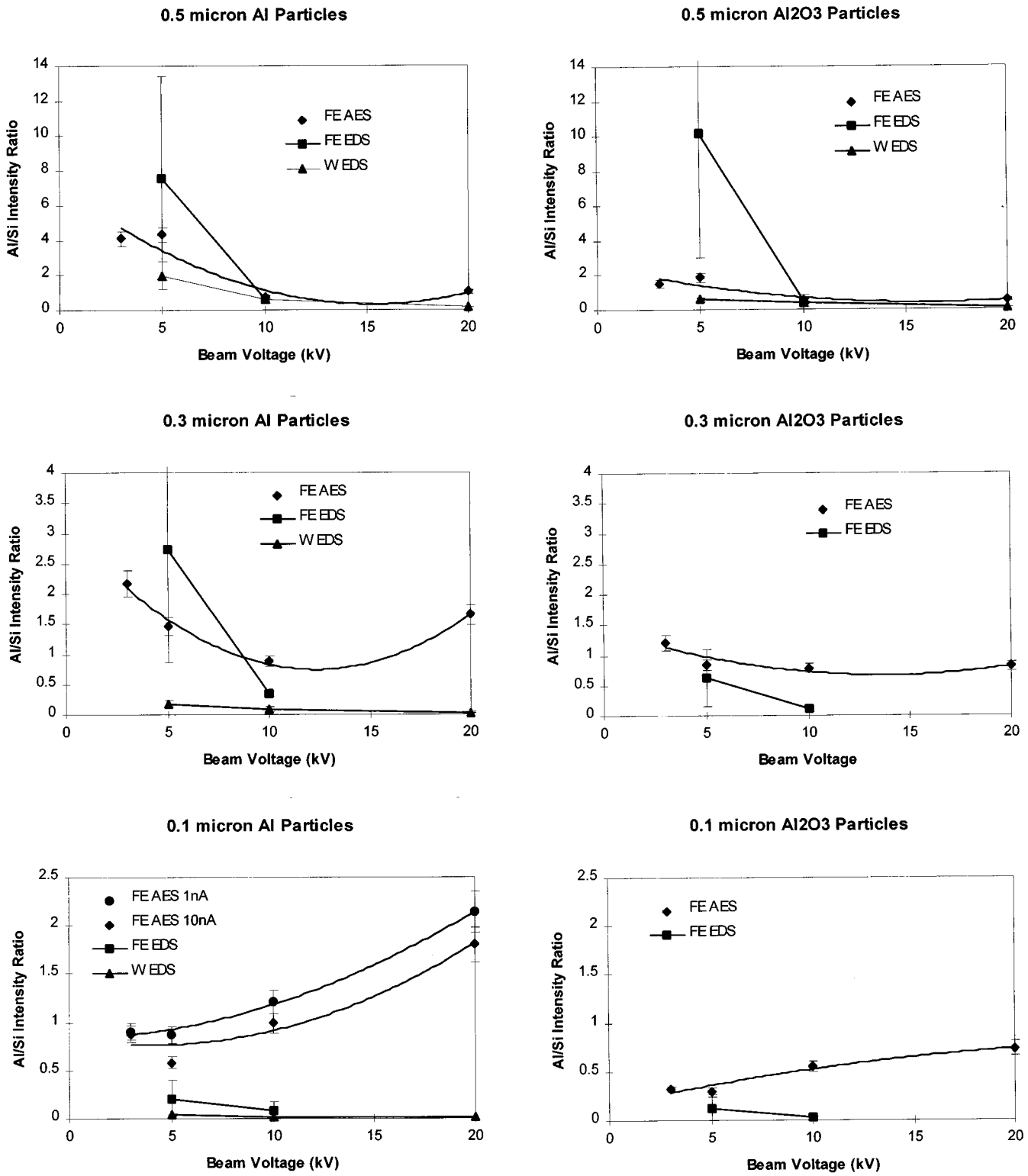

FIG. 5. Plots of average Al/Si intensity ratios for Auger peak to peak heights and EDS peak areas as a function of primary beam voltage for the 0.5-, 0.3-, and 0.1-μm Al particles on Si.

FIG. 6. Plots of average Al/Si intensity ratios for Auger peak to peak heights and EDS peak areas as a function of primary beam voltage for the 0.5-, 0.3-, and 0.1-μm Al_2O_3 particles on Si.

field emission electron gun and a multichannel electron detector. Maintaining a coaxial geometry between the electron column and the electron energy analyzer eliminates any analytical confusion resulting from shadowing of the particles on a surface.

Auger spectra and multiplex data were acquired with primary beam voltages of 20, 10, 5, and 3 kV. These data were acquired in point mode, centered on the particles. The primary beam current was 1–10 nA. Secondary electron images of the particles were obtained at both 1 and 10 nA. Spectra

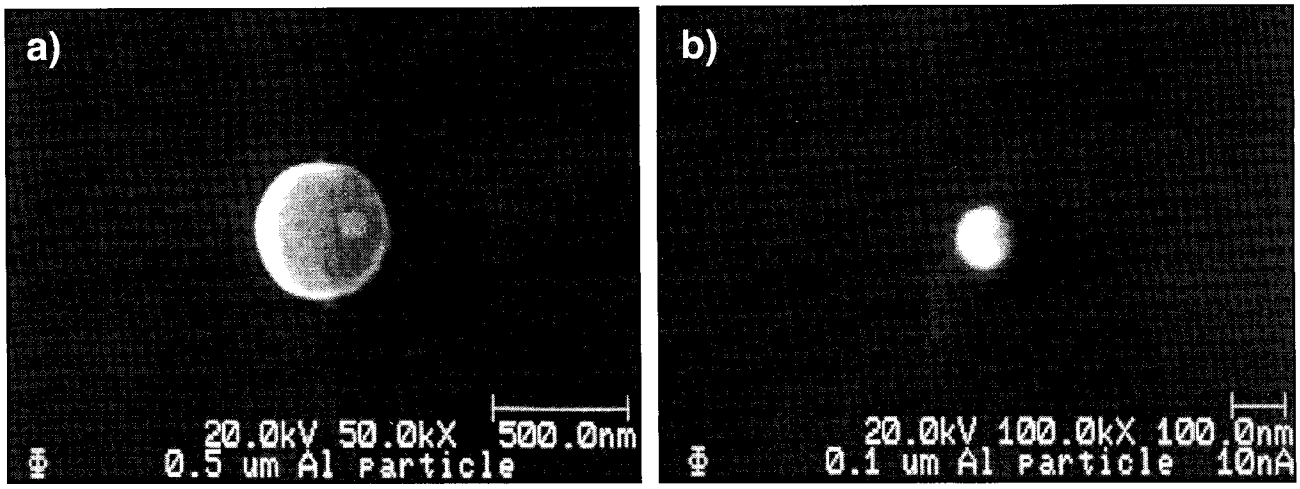

FIG. 7. Secondary electron images of typical particles analyzed by AES. Round or nearly round particles were chosen for Auger analysis. (a) 0.5-μm Al particle and (b) 0.1-μm Al particle.

were acquired on the as-received particles and after a short Ar^+ ion sputter clean. Narrow energy range multiplex spectra were acquired for O, Al, and Si after sputter cleaning to achieve high signal-to-noise ratio data.

Sputter etching was accomplished with a hot filament, differentially pumped, inert gas ion gun. The samples were sputtered for 1 min, were rotated 180° and sputtered for another minute to eliminate any sputter shadowing. The sputter rate was ~50 Å/min in SiO_2. Auger maps were obtained after the sputter clean, using a 20 kV 10 nA primary electron beam.

All the Al particles analyzed with AES were individual round particles and the Al_2O_3 particles were regularly shaped, nearly round particles. Care was taken that either the same particle or particles of comparable size and shape were used for the acquisition of Auger data with different beam

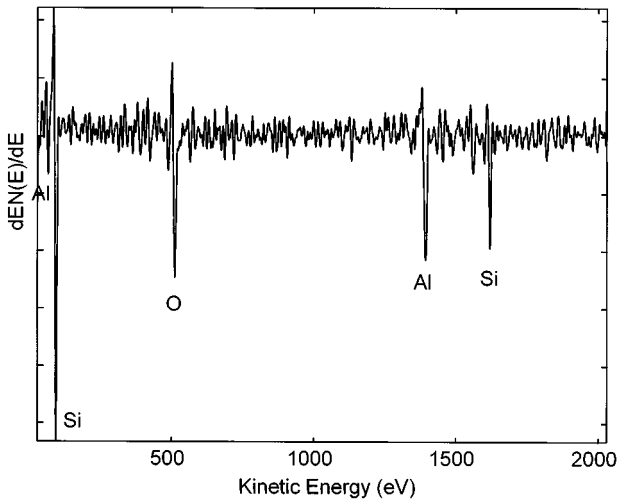

FIG. 8. Auger spectra from a 0.1-μm Al_2O_3 particle acquired in just 10 s using a 20 kV, 10 nA primary electron beam.

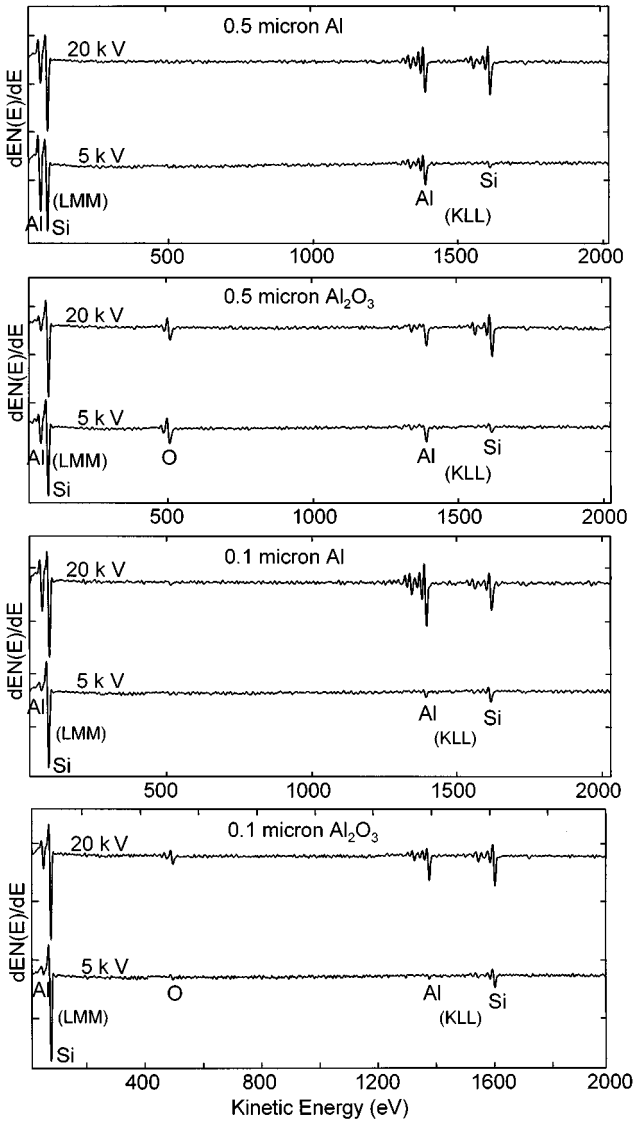

FIG. 9. Auger spectra for the 0.5- and 0.1-μm Al and Al_2O_3 particles after sputter cleaning, acquired with 20 and 5 kV primary beam voltages.

voltages on a specific particle type. Secondary electron images of typical 0.5- and 0.1-μm Al particles are shown in Fig. 7.

B. AES results and discussion

Auger analysis provides rapid identification of the particles' major constituents. This is demonstrated with spectra of the as-received particles which were acquired in just 10 s using a 20 kV 10 nA primary electron beam and from which Al can be readily identified, as shown in Fig. 8. Spectra for the 0.5- and 0.1-μm Al and Al_2O_3 particles after sputter cleaning are shown in Fig. 9. These spectra were signal averaged for 3.33 min, providing rapid analysis with good signal-to-noise ratio. Al is found for all six particle types, with O found for the three oxide particles.

The distinction between Al and Al_2O_3 particles is evident after sputter cleaning, in that spectra from Al_2O_3 particles have significant O, while those from Al particles do not. In many cases it is also possible to distinguish between particles that are Al metal and Al oxide from the Al line shape. An example of this is shown in Fig. 10 for the 20 kV spectra taken from the as-received 0.5-μm Al and Al_2O_3 particles.

Si from the surrounding substrate is also observed in the Auger spectra of the particles. The presence of Si results from primary electrons that are scattered to the Si surface, resulting in the emission of Auger electrons. The relative contribution of the signal from the particle to that from the substrate can be monitored by calculating the Al/Si intensity ratio. To accomplish this, multiplexed data were obtained for the Al and Si *KLL* transitions. These spectra were differentiated and intensities obtained from peak to peak height measurements.

Figures 5 and 6 show plots of the Al/Si intensity ratio as a function of beam voltage for the Al and Al_2O_3 particles. The solid lines associated with the Auger data are included to aid the visualization of trends. In those cases where multiple measurements (two or three) were made under the same analytical conditions, the standard deviation from the average Al/Si ratio was typically on the order of 10% or less. In a few cases, when the particles were characterized on two different 670*xi* Auger systems, the standard deviation was on the order of 20%. Error bars of 10% are included in Figs. 5 and 6 to indicate the expected reproducibility of the Auger measurements.

The Al and Si *LMM* intensities were also measured. However, in every case, the Al/Si *LMM* ratio was less than that for the *KLL* ratios. This occurs because the lower energy *LMM* intensities have a greater contribution of substrate intensity from scattered primary electrons. Primary electrons can travel further, lose more energy, and still excite the *LMM* transitions where they would not excite the *KLL* transitions.

Figures 5 and 6 show that for the 0.5-μm particles the relative Si contribution tends to decrease with decreasing primary beam voltage. Thus, for these particles a beam voltage of 3–5 kV is optimal. This is the expected result, as the lateral extent and total contribution to the Auger intensity

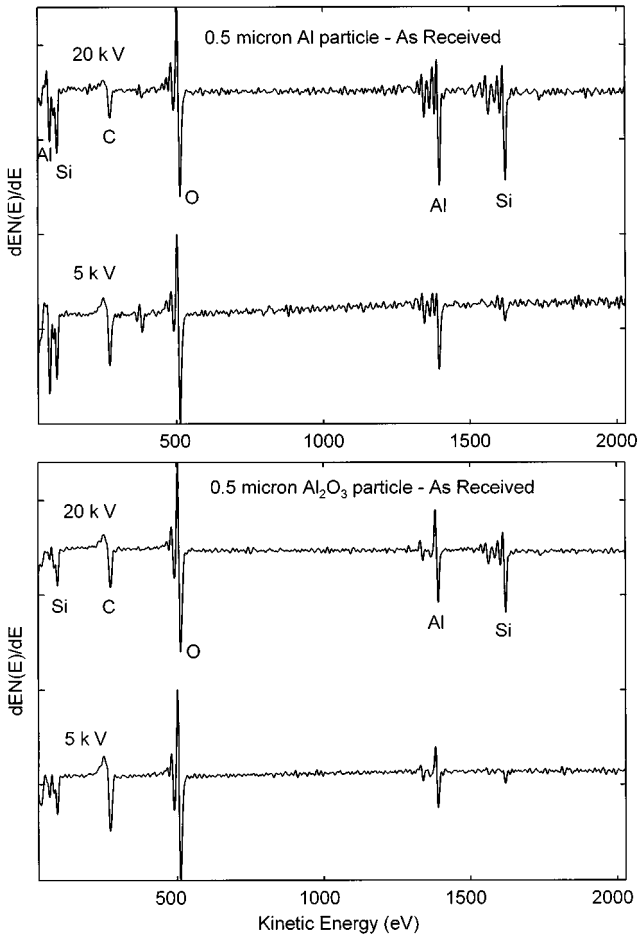

FIG. 10. Auger spectra for the as-received 0.5-μm Al and Al_2O_3 particles acquired with 20 and 5 kV beam voltages. Note that the chemical state of Al is evident in the Al line shape.

due to backscattered electrons have previously been shown to increase with increasing primary beam voltage for flat surfaces[5–7] and larger (>1 μm) particles.[8,9] However, for the 0.3-μm particles, a moderate beam voltage of 10 kV results in *lower* Al/Si ratios. That is, for the 0.3-μm particles, a 10 kV primary beam results in a greater substrate contribution than either 3 or 20 kV. In this case, 20 kV may be preferable

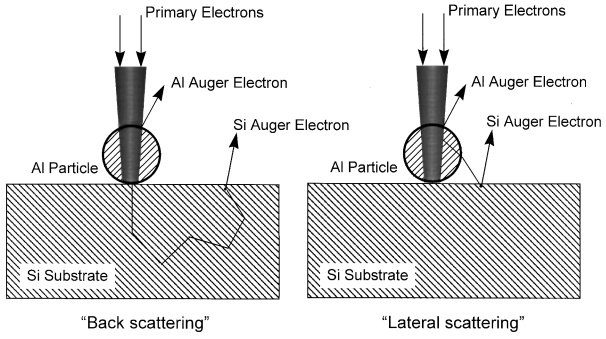

FIG. 11. Schematic diagram of two scattering paths that can result in the excitation of substrate Auger signal with the electron beam incident on a particle.

since the use of a 3 kV beam voltage is less practical for measuring high energy transitions (>1000 eV) such as the Si and Al *KLL*. This is because the Auger yield for higher energy transitions is quite small for low energy primary electrons. For the 0.1-μm particles the largest Al/Si ratio is obtained with a 20 kV primary electron beam. Thus, for the smallest particles, the highest beam voltages are optimal. This result is contrary to that expected for flat samples or large particles.

The effect of beam size on the Al/Si ratio is demonstrated in Fig. 5 for the 0.1-μm Al particles. Measurements were made at both 1 and 10 nA primary beam current, where greater beam currents result in larger beam diameters. The chart shows that, at a given beam voltage, the Al/Si ratio is systematically larger for smaller beam diameters, with the effect more pronounced at higher beam voltages. For larger particles, the difference between 1 and 10 nA had less effect on the Al/Si ratio.

The trends in Al/Si intensity ratios are felt to depend in a complex way on beam size, particle size, and the scattering behavior of the primary electrons, and will be discussed in more detail in a future article. However, a relatively simple consideration of primary electron scattering as a function of primary electron energy can describe the broad differences between the large and small particles. When an electron beam impinges a particle there are two scattering paths that result in the excitation of signal outside the point of contact of the electron beam as illustrated in Fig. 11. One path is the *lateral* scatter of electrons from the primary beam out of the side of the particle and onto the substrate. The second path is excitation due to *backscattered* electrons that result from primary beam electrons that pass through the particle, into the substrate, and reflect back toward the surface.

For the 0.1-μm particles, the variation in Al/Si ratio with beam voltage is thought to result primarily from the *lateral* scatter of primary electrons out the sides of the Al particles, resulting in excitation of Si Auger electrons from the surrounding substrate. At higher beam voltages the primary electrons penetrate directly through the small particles with little scattering within the particle and thus less lateral scattering of primary electrons out the particle sides. At lower beam voltages, the scatter within the small particle is greater, with the result that more primary electrons are laterally scattered out of the particle sides. These laterally scattered primary electrons are more numerous near the substrate surface than are backscattered electrons from within the substrate, and thus contribute a larger substrate Auger signal.

As the particle size increases the scattering results for low primary beam voltages approach those expected for flat samples, where a significant portion of the interaction volume is contained within the particle. At high beam voltages the interaction volume is still large compared to the particle

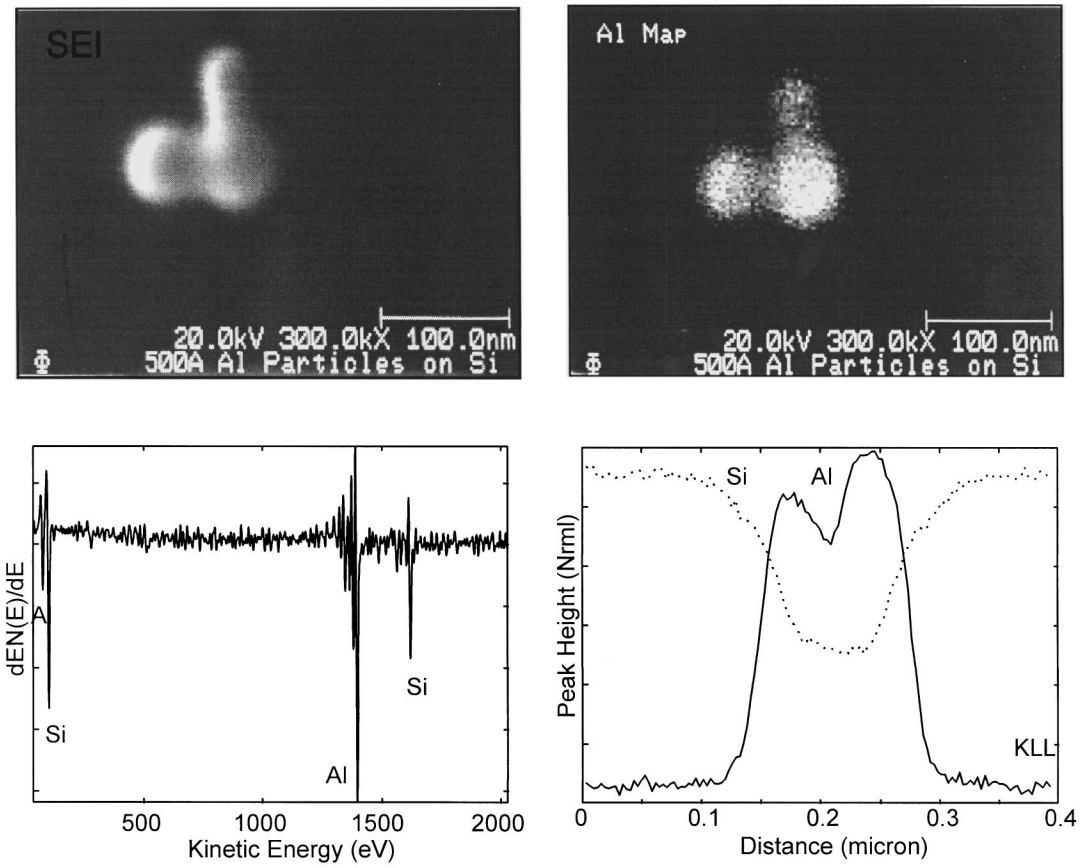

FIG. 12. Secondary electron image and Al Auger map of a trio of ~500 Å Al particles, obtained at an original magnification of 300 000×. The Auger spectrum of the central particle was acquired in 1.8 min. The Al and Si Auger line scans were acquired horizontally across the bottom two particles.

size. Since the 20 kV interaction volume is large compared to all particle sizes considered in this study, the Al/Si intensity ratio is not strongly dependent on particle size at 20 kV. The differences in electron scattering are evident in the Monte Carlo simulations[4] for the 0.5- and 0.1-μm Al particles on Si, shown in Fig. 4.

An additional capability of Auger analysis is the acquisition of high spatial resolution Auger maps of the elements present on the surface. These maps reveal the detailed two-dimensional spatial distribution of the surface components. An example of the ability to obtain Auger maps on small particles is shown for a set of three, roughly 500-Å, Al particles. Figure 12 shows a secondary electron image, Al Auger map, and Al and Si line scans of the 500-Å particles, acquired at an original magnification of 300 000×. An Auger spectrum, obtained in less than 2 min with a 20 kV 10 nA electron beam, clearly identifies the Al particle and is also shown in Fig. 12. The Al Auger map coincides with the secondary electron image (SEI) and has roughly the same spatial resolution as the SEI.

The line scan data and the Auger spectrum are useful for characterizing the spatial resolution of the Al and Si Auger maps and the magnitude of the background silicon signal. The Al signal off the particle is negligible since the particle represents a small fraction of the area excited by backscattered electrons. The Si signal on the particle never reaches zero, as can be seen in the Si line scan and the Auger spectrum. This Si signal is due to the scattering of primary electrons to the surrounding Si substrate surface as described in the previous paragraphs. The line scan shows a larger Al intensity for the center particle. This is due to primary electrons that scatter into the other two particles when the center particle is analyzed. A measurement of the edge profile of the Al line scan indicates that the lateral resolution for Al imag-

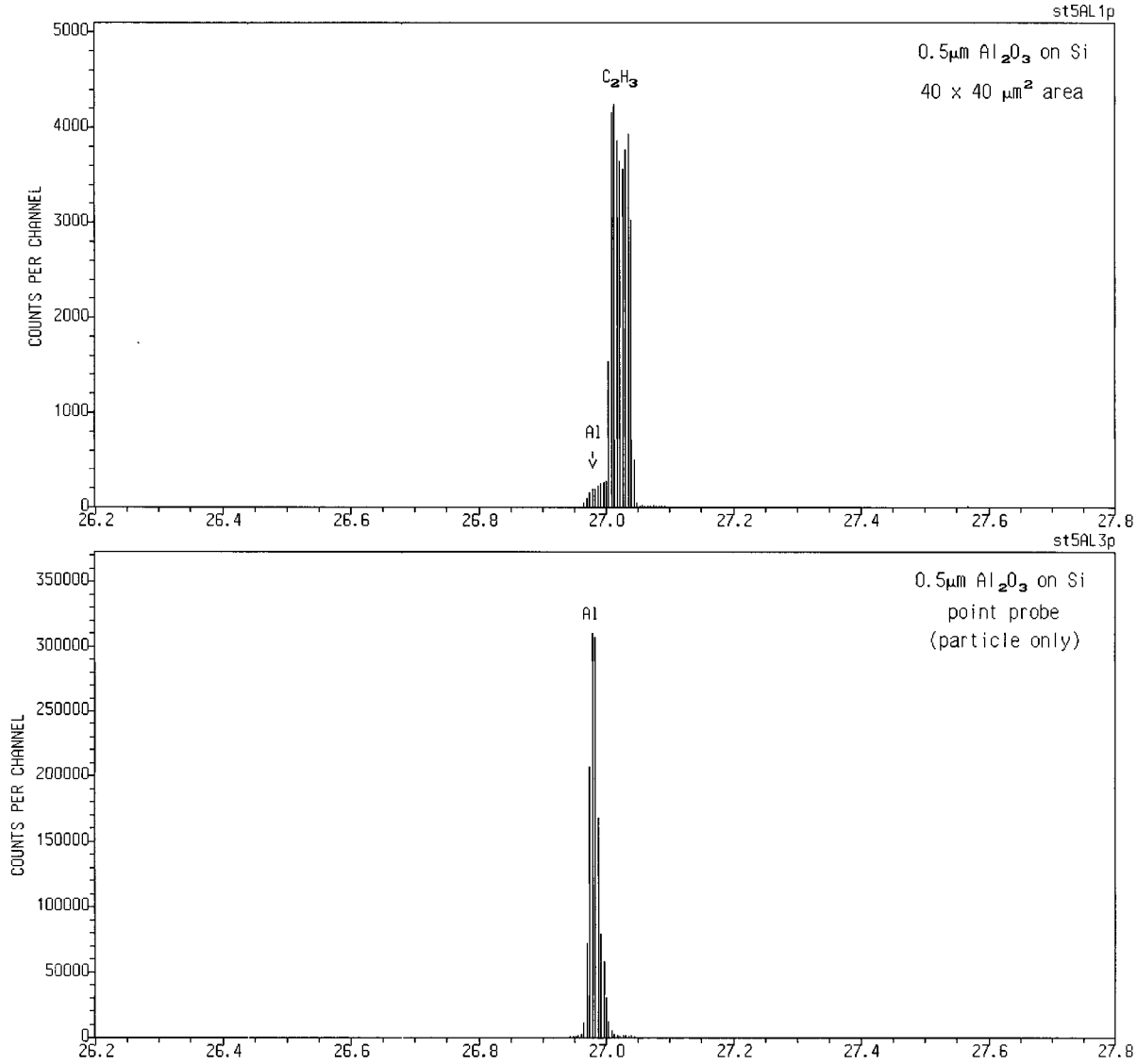

FIG. 13. TOF-SIMS mass spectra illustrating the difference in Al signal on a 0.5-μm Al_2O_3 particle and averaged over a large area. These spectra also illustrate the mass separation of Al and $C_2H_3^+$.

ing is roughly equivalent to the beam size. This is consistent with Monte Carlo simulations for imaging an abrupt element couple.[5]

V. TOF-SIMS ANALYSIS OF Al AND Al_2O_3 PARTICLES ON Si WAFERS

A. TOF-SIMS experiment

TOF-SIMS analysis was performed on a Physical Electronics TRIFT time-of-flight secondary ion mass spectrometer. A pulsed, rastered ^{69}Ga liquid metal ion gun (LMIG) was used as the primary ion source. This ion gun produces short ion bursts to stimulate secondary ion production and is currently capable of achieving pulsed spot sizes down to about 1000 Å at 60 pA instantaneous current. TOF-SIMS provides high sensitivity surface analysis due to its inherent parallel detection capability. Thus, the analytical conditions can be chosen in such a way that practically *all* secondary ions of a given polarity are also detected. This makes it possible to analyze surfaces with minimal primary ion beam damage. Typical ion doses required to perform a TOF-SIMS analysis are on the order of 10^{12} primary ions/cm^2 (static SIMS limit), making it possible to characterize both organic molecular and elemental contaminants.

In these experiments, positive ion TOF-SIMS mass spectra and secondary ion images were acquired with the LMIG operated at 40 pA instantaneous current. The pulse width of the LMIG was reduced to $\sim$ 11 ns in order to permit separation of Al from the organic ion, $C_2H_3^+$, at the same nominal mass. This results in a mass resolution of 1000–2000. Shortening the pulse width has the effect of slightly broadening the primary ion beam, in this case to approximately 2000 Å. The particles were located by acquiring pulsed secondary ion images of Al^+. After completion of the static SIMS analysis,

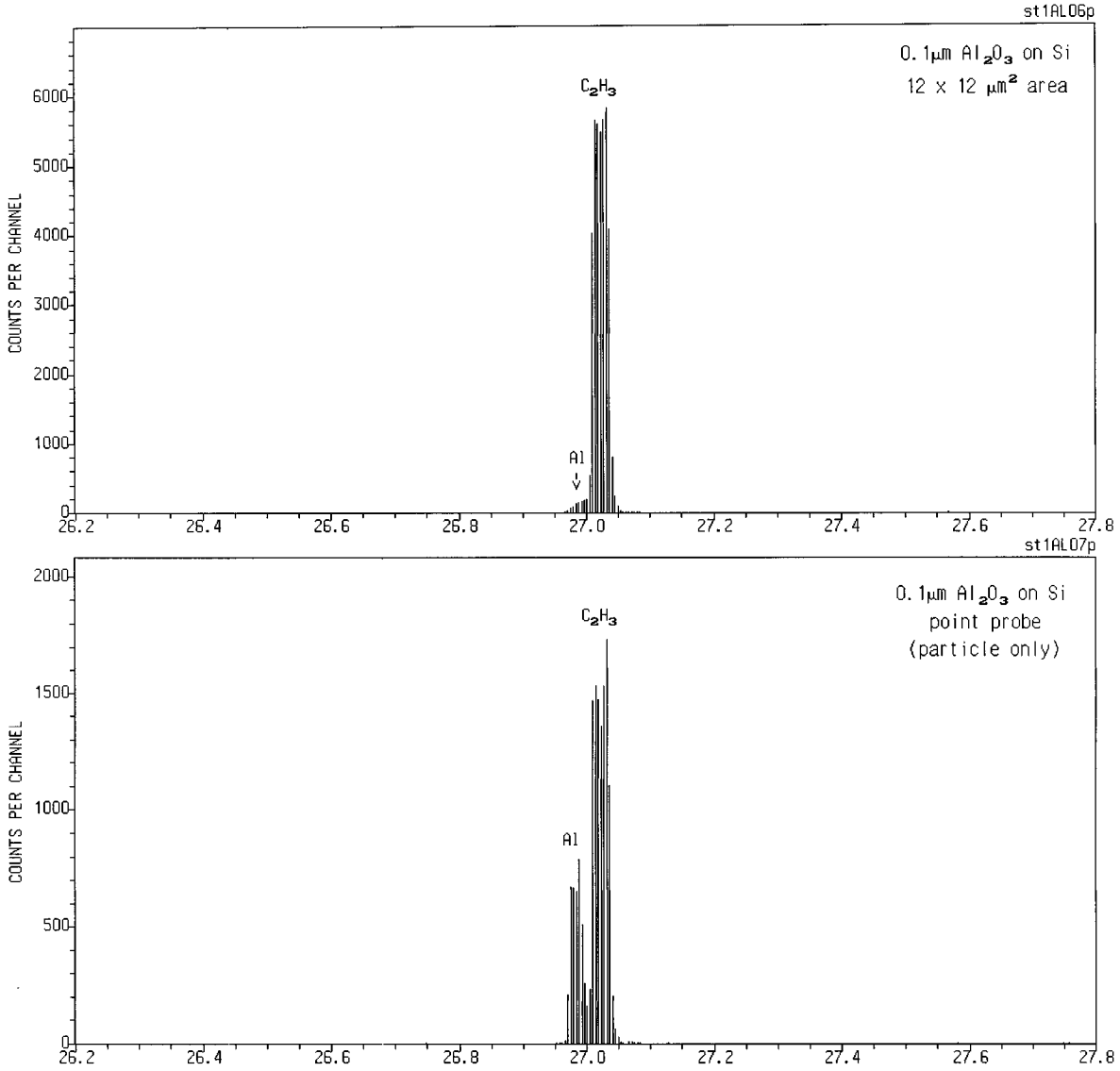

FIG. 14. TOF-SIMS mass spectra illustrating the difference in Al signal on a 0.1-μm Al_2O_3 particle and averaged over a large area. These spectra also illustrate the mass separation of Al and $C_2H_3^+$.

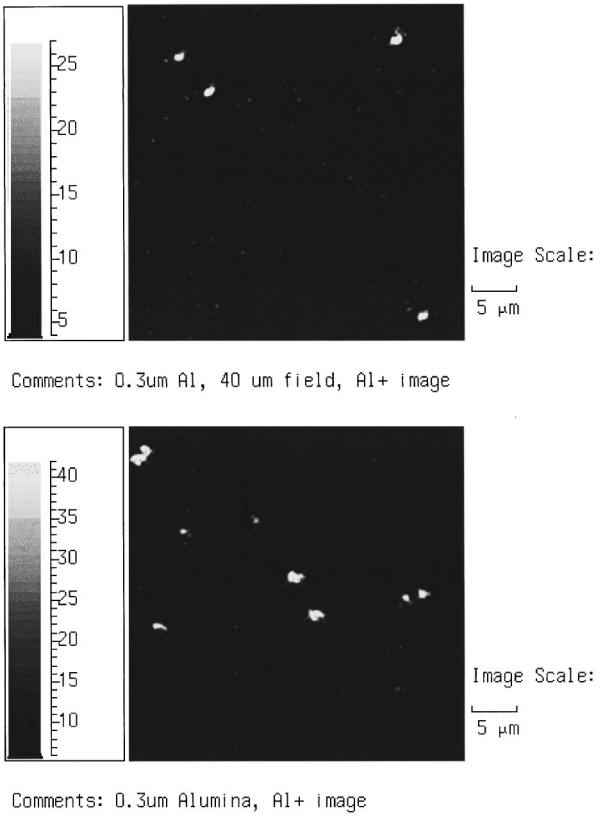

FIG. 15. TOF-SIMS Al maps of 0.3-μm Al and Al_2O_3 particles.

total positive ion images were acquired with the ion beam operated in a continuous mode. Additionally, depth profiles were obtained by focusing the beam on a single particle and monitoring the secondary ion intensities for individual species as a function of time.

B. TOF-SIMS results and discussion

The particles were located and the initial data acquired with the instrument operated in a static SIMS mode, conditions that allow the acquisition of organic molecular information. These conditions would be useful for analysis of

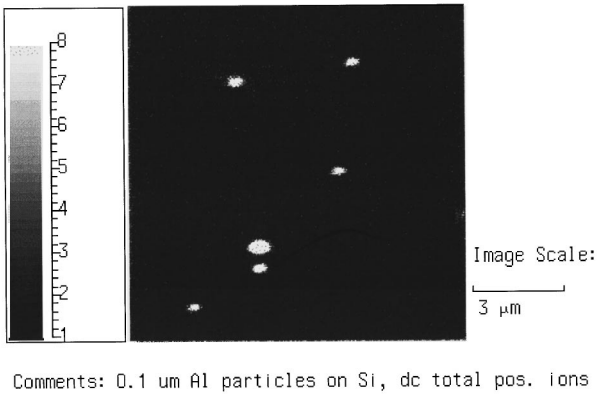

FIG. 16. TOF-SIMS total positive ion image from the 0.1-μm Al particle sample.

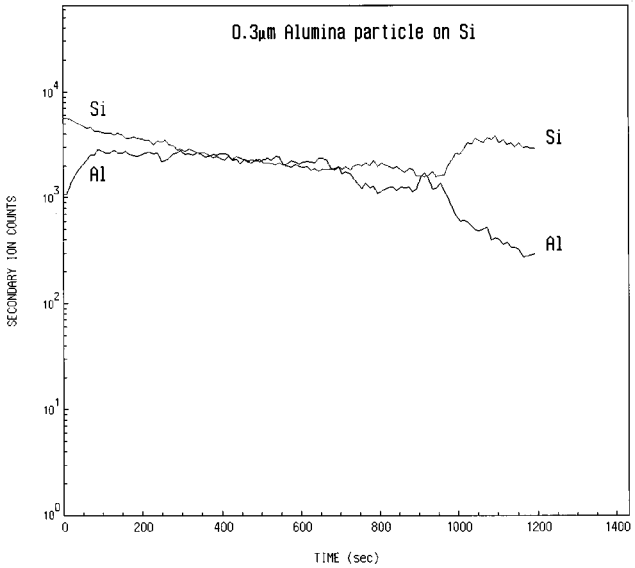

FIG. 17. TOF-SIMS depth profile of a 0.3-μm Al_2O_3 particle.

particles of unknown origin, which may be organic in nature. The difference in Al signal on and off a 0.5- and 0.1-μm Al_2O_3 particle is shown in Figs. 13 and 14, respectively. These spectra also serve to illustrate the mass separation of Al and $C_2H_3^+$. Note that no hyrocarbon is evident for the point probe spectrum of the 0.5-μm particle, while a hydrocarbon is evident for the point probe spectrum of the 0.1-μm particle. This suggests that a hydrocarbon is on the Si wafer but not the particle, and that the area probed by the ion beam is between 0.5 and 0.1 μm.

Because the particles are composed of compounds having high secondary ion yields (Al_2O_3 and the surface oxide on Al), maps of the Al^+ distribution were most useful to locate the particles. Al maps of 0.3-μm Al and Al_2O_3 particles are shown in Fig. 15. Total ion maps and Si ion maps generally

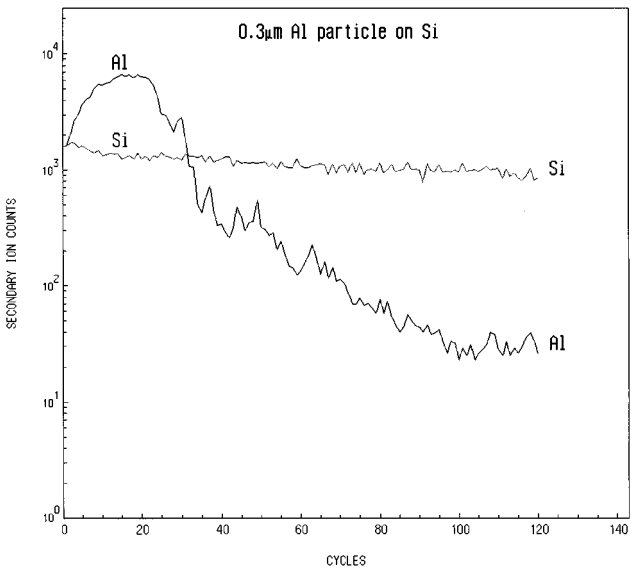

FIG. 18. TOF-SIMS depth profile of a 0.3-μm Al particle.

resulted in less useful images for particle location when obtained in under static SIMS conditions. However, both ion-induced secondary electron images and total positive ion maps were able to locate the particles when they were obtained using a continuous ion beam that would destroy organic molecular information on the surface. Since attempts were made to analyze the particles under static SIMS conditions, these images were not acquired until after the particles were located. Figure 16 shows a total positive ion image from the 0.1-μm Al particle sample.

In addition to locating particles on each of the samples, a second goal of this work was to differentiate the Al and alumina particles. However, under static SIMS conditions, the TOF-SIMS sampling depth of 1–3 monolayers (approximately 10 Å) would not penetrate beyond the native oxide layer of aluminum, meaning that surface spectra from the two types of particles are quite similar.

Al and Al_2O_3 could be differentiated by performing an analysis at depth in the samples. This was accomplished by obtaining depth profiles with the LMIG focused on single Al_2O_3 and Al particles, as shown in Figs. 17 and 18. For the alumina samples, the particle oxide produced a relatively flat Al^+ profile. However, in the case of the Al samples, oxide enhancement of the Al^+ signal was lost below the native oxide, and the Al^+ signal intensity decreased significantly at that point.

VI. CONCLUSIONS

The selection of appropriate analysis methods depends on the application. One immediate advantage of the electron beam imaging techniques, SEM/EDS and AES, for small particle characterization is the ability to obtain high spatial resolution secondary electron images. This is of obvious utility in locating the particles, characterizing their shape and defining an appropriate area for analysis. While all three techniques have imaging capabilities, Auger analysis allows compositional mapping of defects at the highest magnification. The surface sensitive techniques, AES and TOF-SIMS, provide the added capability of characterizing nonparticulate surface contamination. For very large particles, EDS, with its greater analyzed volume, is able to measure the bulk of the particle. TOF-SIMS is the only method capable of providing detailed analysis of organic contamination.

Although AES, TOF-SIMS, and SEM/EDS are all capable of nonquantitative analysis of sub-0.5-μm particles on unpatterned silicon wafers, distinguishing Al from Al_2O_3 is considerably more difficult, especially for the smallest particles. In this study, AES most clearly distinguished the oxide from metal for all particle sizes. Characterization of particles on patterned wafers, with multicomponent layered structures, is expected to complicate EDS analysis more than AES or TOF-SIMS.

Presented at the 42nd National Symposium of the American Vacuum Society, Minneapolis, MN, 16–20 October 1995.

[1]A. Diebold, *A Comparison of Particle Composition Analysis Methods*, Sematech Technology Transfer Document No. 95042788A-TR (Sematech, Austin, TX, 1995).
[2]*National Technology Roadmap for Semiconductors* (Semiconductor Industry Association, San Jose, CA, 1994).
[3]A. Diebold, *Metrology Roadmap: A Supplement to the National Technology Roadmap for Semiconductors*, Sematech Technology Transfer Document No. 94102578A-TR (Sematech, Austin, TX, 1995).
[4]Electron Flight Simulator™ Version 2.0, Small World, P.O. Box 25284, San Mateo, CA 94402.
[5]M. M. El Gomati, A. P. Janssen, M. Prutton, and J. A. Venables, Surf. Sci. **85**, 309 (1979).
[6]M. M. El Gomati and M. Prutton, Surf. Sci. **72**, 485 (1978).
[7]N. M. Glezos and A. G. Nassiopoulos, Surf. Sci. **254**, 309 (1991).
[8]R. R. Olson, L. A. LaVanier, and D. H. Narum, Appl. Surf. Sci. **70/71**, 266 (1993).
[9]K. D. Childs, L. A. LaVanier, and K. P. Muller, in *Proceedings of the Third International Conference on Materials and Process Characterization for VLSI, 1994*, edited by X. F. Zong, M. K. Balazs, and J. J. Wang (Asia-Pacific Microanalysis Association, Shanghai, China, 1994), pp. 16–22.